JOURNAL OF GEOPHYSICAL RESEARCH, VOL. 106, NO. B10, PAGES 21,897–21,916, OCTOBER 10, 2001

Seismic wave observations with the Global Positioning System

Rosanne M. Nikolaidis, Yehuda Bock, Paul J. de Jonge, Peter Shearer, Duncan Carr Agnew, and Matthijs Van Domselaar

Cecil H. and Ida M. Green Institute of Geophysics and Planetary Physics
Scripps Institution of Oceanography, La Jolla, California, USA

Abstract. We describe the direct measurement of ground displacement caused by the Hector Mine earthquake in southern California (M_w 7.1, October 16, 1999). We use a new method of instantaneous positioning, which estimates site coordinates from only a single epoch of Global Positioning System (GPS) data, to measure dynamic as well as static displacements at 24 stations of the Southern California Integrated GPS Network (SCIGN), with epicentral distances from 50 to 200 km. For sites outside the Los Angeles basin the observed displacements are well predicted by an elastic half-space model with a point shear dislocation; within the sedimentary basin we observe large displacements with amplitudes up to several centimeters that last as long as 3-4 min. Since we resolve the GPS phase ambiguities and determine site coordinates independently at each epoch, the GPS solution rate is the same as the receiver sampling rate. For the SCIGN data this is 0.033 Hz (once per 30 s), though sample rates up to 2 Hz are possible with the SCIGN receivers. Since the GPS phase data are largely uncorrelated at 1 s, a higher sampling rate would offer improved temporal resolution of ground displacement, so that in combination with inertial seismic data, instantaneous GPS positioning would in many cases significantly increase the observable frequency band for strong ground motions.

1. Introduction

Geodetic observation of Earth's response to tectonic motion involves repeated measurement of the position of surface points. Data from permanent Global Positioning System (GPS) receivers provide a record of ground motion that is stable over long periods and very effective in measuring coseismic and postseismic deformation. Continuous GPS was first used to measure coseismic displacements following the M_w 7.3 Landers, California, earthquake in 1992 with data from the Permanent GPS Geodetic Array (PGGA) [*Bock et al.,* 1993; *Blewitt et al.,* 1993]. Further analysis led to the observation of transient postseismic motion throughout the region in the following months [*Bock et al.,* 1997]. Coseismic and long-period postseismic deformation is now routinely observed by the Southern California Integrated GPS Network (SCIGN) (http://www.scign.org) and other continuous GPS networks spanning plate boundaries, for example, the Japanese Geographical Survey Institute nationwide GPS Earth Observation Network (GEONET) array [*Miyazaki et al.,* 1998]. Coseismic displacements are typically estimated from daily (or subdaily) GPS solutions, in which GPS phase measurements are combined in 24-hour (or several hour) batches. With this type of processing the coseismic response is taken to be an instantaneous step function.

However, this static displacement is only part of the effect of fault rupture; much larger, if more temporary, displacements are produced by the elastic waves radiated from the source. These are usually measured with inertial sensors which are sensitive to acceleration; long-period displacements can be obtained from such data only by double integration. At lower and lower frequencies this multiplies the signal, and any noise, by increasing amounts. Despite these difficulties, static ground displacements have been computed from digital strong-motion data, both in laboratory tests [*Iwan et al.,* 1985] and from data near the 1985 M_w 8.1 Michoacan, Mexico, earthquake [*Anderson et al.,* 1986], from broadband data, for example, near the the 1994 M_w 8.2 Bolivian earthquake [*Ekstrom,* 1995; *Jiao et al.,* 1995; *Vidale et al.,* 1995], and also from force balance accelerometer data near the 1998 M_w 5.1 San Juan Bautista, California, earthquake [*Urhammer et al.,* 1999].

Here, rather than extracting low-frequency information from seismic data, we examine high-frequency displacements from geodetic data. We demonstrate the use of instantaneous positioning with GPS [*Bock et al.,* 2000] to measure ground displacements from the Hector Mine earthquake in southern California (October 16, 1999), which had moment magnitude 7.1 [*U.S. Ge-*

Paper number 2001JB000329.
0148-0227/01/2001JB000329$09.00

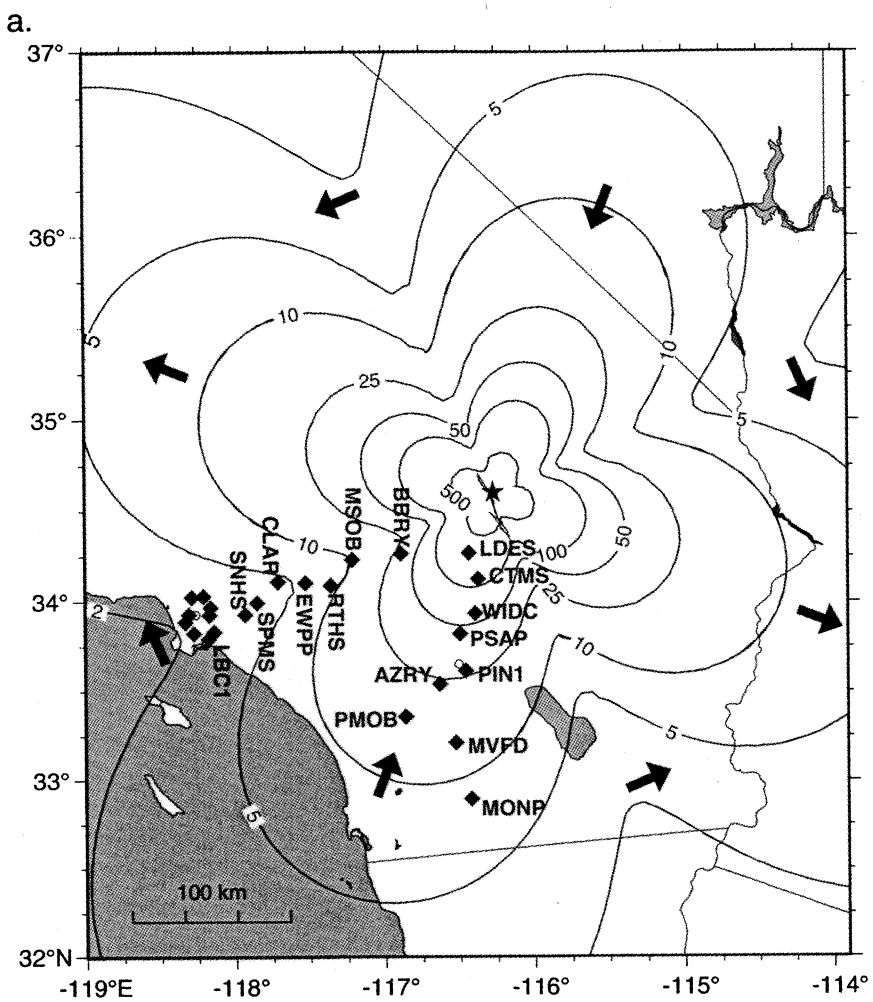

Figure 1. Southern California, showing the location of the October 16, 1999, M_w 7.1 Hector Mine earthquake epicenter (star) and fault rupture. Magnitude (contours (in millimeters)) and direction (arrows) of the (a) static horizontal displacement and (b) maximum horizontal displacement, including both static and dynamic components, for the modeled source (see text for details). Diamonds show the 25 SCIGN sites used in this study (Table 1). (c) Locations of the SCIGN sites in the Los Angeles basin and the three TriNet strong motion sensors (open circles), LAS, DOW, and LBG.

ological Survey, et al., 2000]. We present displacements for a subset of SCIGN sites (Figure 1) with epicentral distances ranging from 53 km to 205 km (Table 1). Because the vertical component of the GPS solutions is generally several times noisier than the horizontal, we discuss only horizontal displacements. We processed the GPS data independently for each sample to generate displacement time series at the receiver sampling rate, in this case every 30 s.

With this sampling frequency and errors of several millimeters (Table 1) we observe both the permanent deformation and the dynamic ground displacements from radiated seismic waves. For sites outside the Los Angeles basin the displacements observed with GPS agree reasonably well with a simple synthetic seismogram. Within the Los Angeles basin the GPS displacements are much larger (amplitudes up to several centimeters) and longer lasting. This is consistent with nearby strong motion data, which show the effect of basin resonance.

2. GPS Seismometer

An inertial seismometer relies on a suspended mass and measures the relative motion between the mass and the instrument frame. Such a system is sensitive only to ground accelerations and can provide displacement only indirectly. GPS receivers, on the other hand, record the displacement between the ground station and the satellites directly and without saturation. Of course, the primary disadvantage of using GPS as a seismometer is that the sensitivity to seismic ground motion, while flat over its observable range, is not nearly as good as that of seismic instruments.

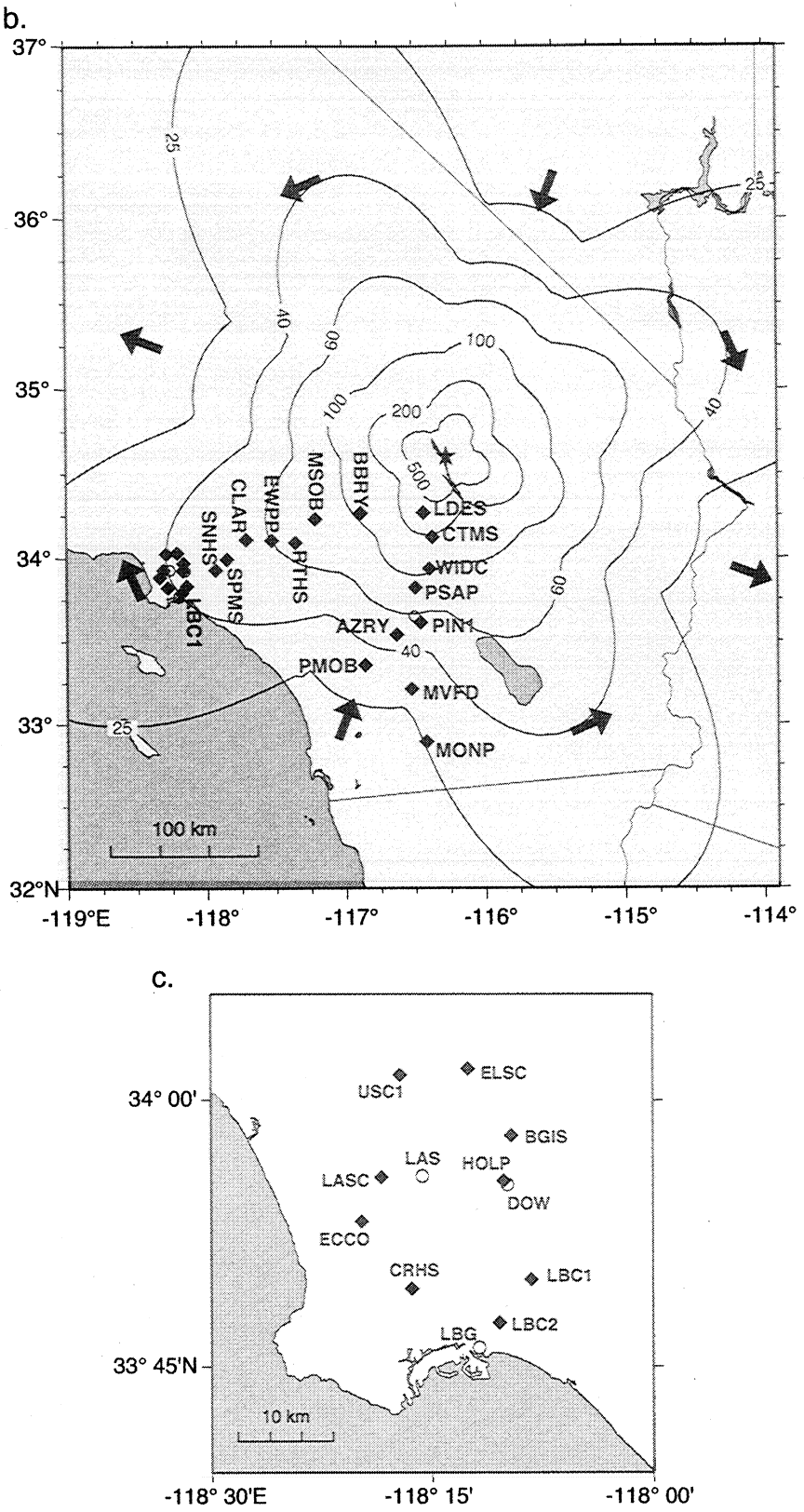

Figure 1. (continued)

The SCIGN receivers are capable of sampling at 2 Hz, and other GPS receivers can sample at rates of up to 20 Hz. A subset of the Japanese GEONET array receivers (118 of the 889 receivers as of April 1997) operate at a 1-Hz sampling rate [*Miyazaki et al.*, 1998]. The 1-Hz data are stored in buffers and resampled at 30 s, unless a large seismic event occurs, in which case the 1-Hz data from sites close to the epicenter are stored for later analysis. Universidad Nacional Autónoma de México is currently installing a 10-station continuous

Table 1. Location and Scatter of Single-Epoch Data

Site	Location	Latitude, °N	Longitude, °E	Epicentral Distance, km	Single-Epoch Scatter,[a] mm	
					North	East
LDES	Landers Elementary School	34.27	−116.43	39	...	...
CTMS	La Contenta Middle School	34.12	−116.37	53	2.8	2.4
WIDC	Wide Canyon	33.93	−116.39	74	3.9	3.3
PSAP	Palm Springs Airport	33.82	−116.49	88	3.4	3.3
PIN1	Piñon Flat	33.61	−116.46	110	3.7	3.7
AZRY	Anza	33.54	−116.63	121	3.5	3.8
PMOB	Palomar Observatory	33.36	−116.86	147	6.1	5.4
MVFD	Montezuma Valley	33.21	−116.53	155	6.1	5.8
MONP	Monument Peak	32.89	−116.42	189	6.6	6.5
BBRY	Big Bear Road Yard	34.26	−116.88	67	3.4	3.8
MSOB	Mountain Skies Observatory	34.23	−117.21	95	5.7	5.0
RTHS	Rialto High School	34.09	−117.35	114	4.9	5.8
EWPP	Etiwanda Power Plant	34.10	−117.53	127	4.6	5.7
CLAR	Claremont	34.11	−117.71	142	4.9	5.9
SPMS	South Pointe Middle School	33.99	−117.85	159	5.4	6.0
SNHS	Sonora High School	33.93	−117.93	169	5.5	6.4
LBC1	Long Beach	33.83	−118.14	191	6.9	8.3
LBC2	Long Beach	33.79	−118.17	196	7.0	8.6
CRHS	Carson High School	33.82	−118.27	202	7.2	8.7
ECCO	El Camino College	33.89	−118.33	204	7.4	9.3
LASC	Los Angeles Southwest College	33.93	−118.31	200	7.1	8.8
USC1	University of Southern California	34.02	−118.29	195	7.7	9.4
ELSC	East L.A. Science Center	34.03	−118.21	188	7.5	9.5
BGIS	Bell Gardens Intermediate School	33.97	−118.16	186	7.4	9.0
HOLP	Hollydale	33.92	−118.17	189	9.1	11.3

[a] Scatter is based on the robust interquartile range (IQR) statistic, defined as the difference between its 75th and 25th percentiles. Assuming normal distribution of the coordinate residuals, the standard deviation would be 74% of the IQR. Thus the values shown correspond to the IQR times 0.74.

GPS array in Mexico with GPS receivers that sample at a 10-Hz rate and are collocated with broadband seismometers (S. K. Singh, V. Kostogolov, and J. Pacheco, personal communication, 2000).

The ability of the GPS receiver to track very high frequency ground motion depends on the time correlation of the individual phase measurements, which may be introduced through smoothing internal to the receiver, and on the averaging interval imposed by the bandwidth of the receiver's phase-tracking loop. We expect that the averaging interval for each phase observation must be less than the maximum receiver sampling rate (e.g., 0.5 s in the case of the Ashtech Z-XII). The time correlation of GPS measurement are best studied using zero-baseline tests in which orbit, multipath, and atmosphere errors are eliminated through double-differencing, so that residual correlations must be induced by receiver noise.

The independence of measurements from the Ashtech Z-XII receivers (the type used in the SCIGN array) has been studied using zero-baseline tests with 1-Hz sampling [*Tiberius,* 1999; *Bona,* 2000]. *Tiberius* [1999] showed that the L2-phase residuals are essentially white noise even at 1-s intervals. *Bona* [2000] concluded that the L1 phase residuals are uncorrelated at 1 s but that the L2 phase residuals are somewhat correlated at time lags of <4 s. Likewise, *Ge et al.* [2000] performed a zero-baseline test with two Leica CRS1000 receivers operating at 10 Hz and found that the L1 phase residuals are independent at 10 Hz and that the L2 phase residuals are only partially independent at 10 Hz but fully independent at 1 Hz. Thus it should be possible to take largely independent measurements of ground motion with these types of receivers at rates of at least 1 Hz.

Gourevitch [1996] demonstrated the ability of an Ashtech Z-XII receiver to track a large transient in ionospheric propagation delay of >1 m over 10 s, or, equivalently, a 10 cm/s change. This indicates that the dynamic response of the Ashtech Z-XII receiver is probably adequate for tracking seismic ground motions with amplitudes of several centimeters. Other experiments have been designed specifically to test the ability of GPS receivers to sense the sort of large-amplitude, periodic signals that might occur with a large seismic event. To simulate earthquake vibrations, *Hirahara et al.* [1994] placed a roving GPS antenna on a mechanical slider that oscillated horizontally with an amplitude of 15 cm

at periods of 25-300 s. They employed Ashtech Z-XII receivers running at 1 Hz, a base station 160 km away, and a kinematic analysis to recover the displacement signal with an accuracy of 1-2 cm every second. *Ge* [1999] executed a similar experiment with two Leica CRS1000 receivers running at 10 Hz. In their study the slider oscillated with frequencies of 2.3 Hz and 4.3 Hz and an amplitude of up to 12.7 mm, and the vibrations were recognizable in both time and frequency domains in both horizontal and vertical directions.

In several instances, GPS has been used to measure ground motions associated with large seismic events. Data collected at four continuous PGGA sites during the 1994 M_w 6.7 Northridge earthquake were analyzed by *vanDam et al.* [1994] to determine relative positions every 30 s. They showed that the sense of coseismic shaking was consistent with seismic data. *Hatanaka et al.* [1994, 1995] and *Miyazaki et al.* [1996] investigated the ground motions from three large earthquakes in Japan (the 1994 M_w 8.2 Hokkaido-Toho-Oki earthquake, the 1994 M_w 7.7 Far-Off-Sanriku earthquake, and the 1995 M_w 6.8 Kobe earthquake) using 30-s GPS data and were able to identify the P wave arrivals over horizontal noise levels of a few centimeters. *Tada et al.* [1997] and *Miyazaki et al.* [1998] analyzed 1-Hz data collected by the GEONET array during the 1996 M_w 6.7 Hyuga-Nada earthquake. The high-rate GPS data allowed identification of both P and S wave arrivals and agreed well with both theoretical seismograms and numerically integrated accelerometer data.

In each of these studies a kinematic analysis was used to estimate site displacements. This processing technique relies on the initial resolution of ambiguities using at least several minutes of data followed by the identification and repair of cycle slips, or reinitialization of ambiguities. For coseismic (static and dynamic) applications, data must be edited carefully to avoid mistaking cycle slips for ground motion. Moreover, it is more likely for a GPS receiver that is designed to measure static displacements to experience cycle slips during a period of intense shaking. Furthermore, standard kinematic analysis is limited to distances of less than roughly 10 km, unless performed in a postprocessing mode. Instead of a kinematic processing approach we use instantaneous GPS positioning [*Bock et al.*, 2000], in which ambiguities are resolved individually at each measurement epoch thereby making cycle slips irrelevant. In this study the technique is implemented in postprocessing mode; however, instantaneous GPS positioning can also be used to track receiver motions in real time.

3. Single-Epoch GPS Observations

Instantaneous GPS positioning, as described by *Bock et al.* [2000], provides relative displacement estimates for distances up to several tens of kilometers, with subcentimeter precision and with solution rates as high as the receiver sampling rate. For each epoch of GPS dual-frequency phase and pseudorange measurements, we resolve the integer-cycle phase ambiguities and estimate the three-dimensional site coordinates. We apply the technique, at a 30-s solution rate, to data collected by the SCIGN network in the 8-hour interval centered on the Hector Mine rupture time (day 289 of 1999, 0946:44 UTC). We held fixed the satellite orbits and Earth orientation parameters to the International GPS Service (IGS) values (http://igscb.jpl.nasa.gov).

We selected sites along two different profiles, one trending roughly north-south and one trending roughly east-west into the Los Angeles basin, as well as a cluster of sites in the Los Angeles basin (Figure 1c). Adjacent sites are up to 35 km apart, an acceptable distance for single-epoch ambiguity resolution. Individual baseline adjustments are then summed along the profiles and added to the position of the site (Landers Elementary School (LDES)) closest to the epicenter. By doing this, we can evaluate the displacements at sites up to a few hundred kilometers from the rupture, all with respect to a common reference (Figure 2).

Because the data are not Gaussian, we use the median and interquartile range (IQR) to characterize the central value and the scatter of the single-epoch coordinate solutions (Table 1). The IQR of a data sample is the difference between its 75th and 25th percentiles and is ~1.3 times the standard deviation for Gaussian data. We cleaned the coordinate solutions using an edit criteria of 3 times the IQR. To prevent exclusion of data possibly affected by the earthquake, data within 10 min of the earthquake origin time were not cleaned.

Single-epoch coordinate solutions are highly sensitive to errors that vary with satellite geometry. We have improved the signal-to-noise ratio in our data by implementing a filter designed to reduce noise with a sidereal day repeat period. This class of noise, which we refer to as "multipath" noise, includes effects of signal attenuation, signal diffraction, antenna phase center variations, diurnal monument variations, and, most predominantly, signal multipath. We modified the algorithm described by *Bock et al.* [2000], in which the multipath signal for a given day is estimated as the weighted mean in a sliding 3-day window and then subtracted from the middle day. Instead, we computed the multipath signal for the earthquake day (289) as the weighted mean of the daily signals on the three previous days (286-288) and then subtracted this from the coordinate time series for day 289; this assures that the multipath estimate is not affected by strong motion or postseismic deformation. This correction reduced the coordinate scatter by 6-45%, compared with the uncorrected data, in each of the time series of single-epoch solutions. The horizontal precision of the resulting single-epoch solutions ranges from ~3 to 10 mm (Table 1). Because of increased differential atmospheric refraction over greater distances [*Bock et al.*, 2000], displacement data incorporating longer baselines (e.g., Montezuma Valley

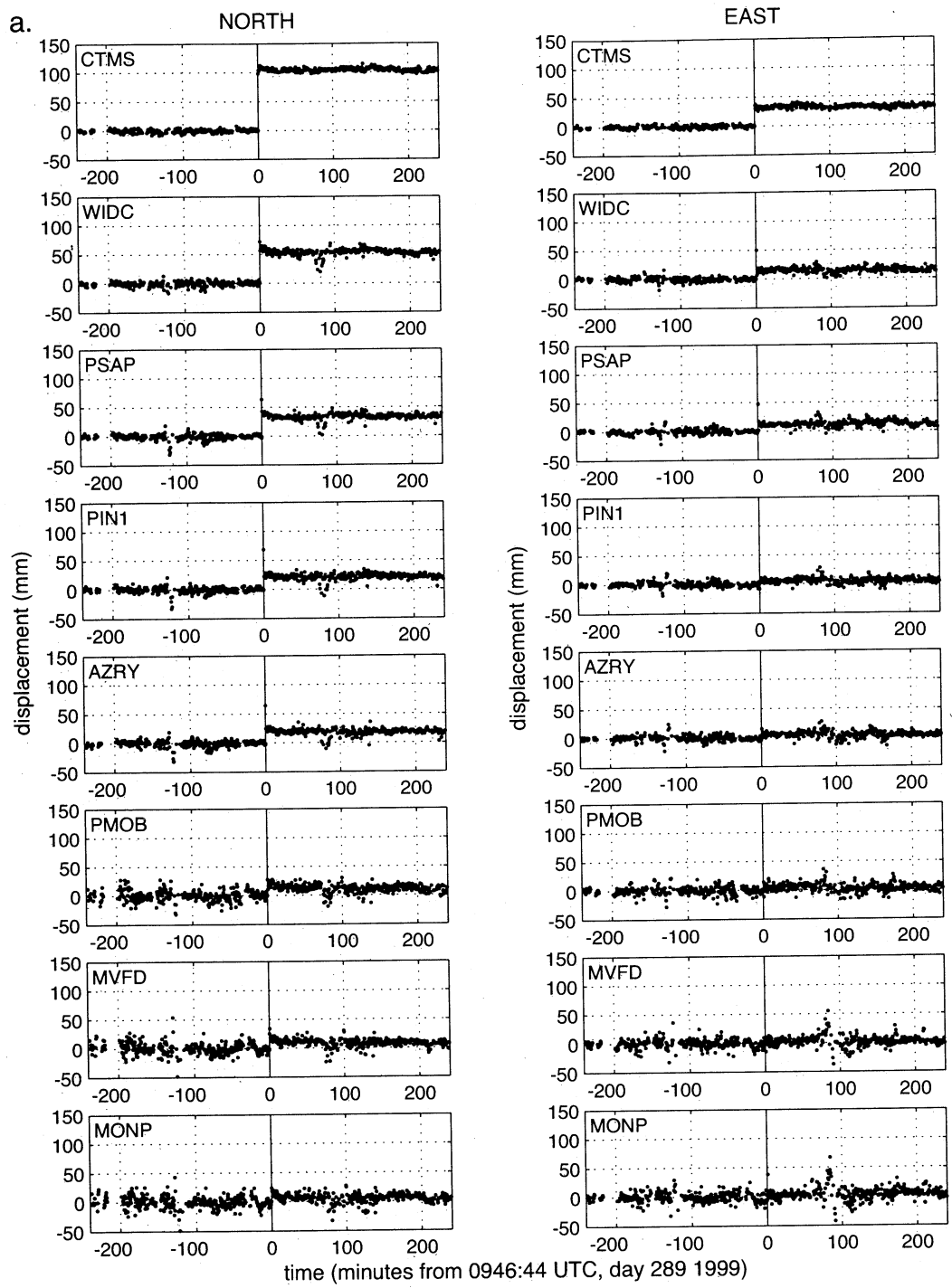

Figure 2. North and east displacements of the (a) north-south profile, (b) east-west profile, and (c) Los Angeles basin sites relative to the preseismic medians. Time is minutes relative to the Hector Mine earthquake (0946:44 UTC, day 289, 1999 (vertical line)). Sites are in order of (top) closest to (bottom) farthest from the epicenter in Figures 2a and 2b, and clockwise from LBC2 in Figure 2c. The GPS sample rate is 0.033 Hz (1/(30 s)). Individual baseline adjustments are summed along each profile and added to the position, with respect to the International Terrestrial Reference Frame (ITRF97) [*Boucher et al.*, 1997], of the closest site (LDES) to the epicenter. The LDES position before and after the earthquake is estimated through a combination of two weeks of daily batch coordinate solutions. All data have been cleaned using an edit criteria of 3 times the interquartile range, and the sidereal periodic multipath noise has been removed as described in the text.

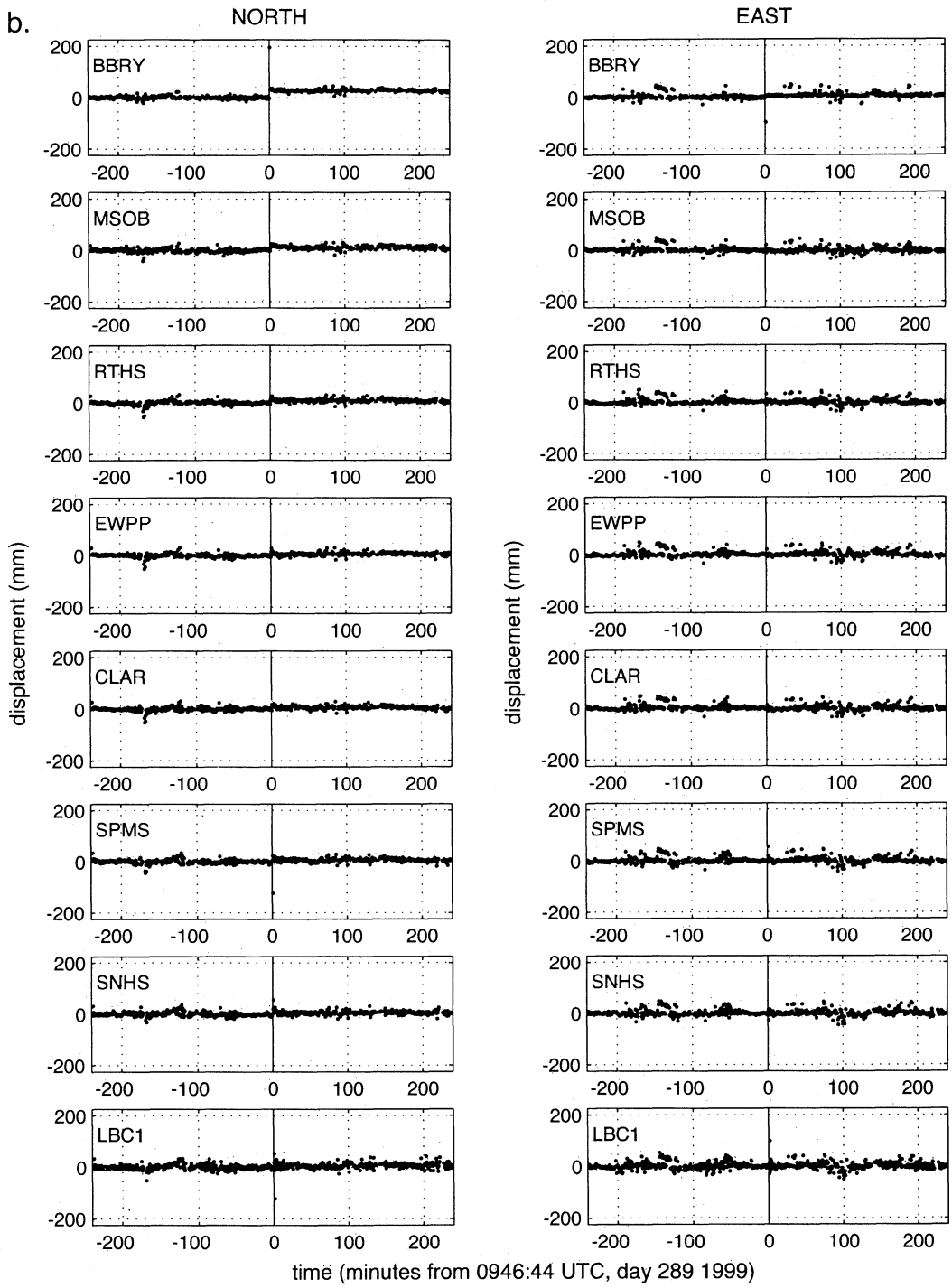

Figure 2. (continued)

(MVFD) and Monument Peak (MONP)) have larger scatter than data made up of only shorter baselines (e.g., La Contenta Middle School (CTMS)).

4. Static Displacement

To present the instantaneous positioning results with respect to a common reference point, we fixed the pre- and post-seismic coordinate positions at LDES to those obtained by the analysis of 2 weeks of daily solutions, each based on 24 hours of GPS data. We performed daily weighted least squares adjustments of coordinates for a regional network of SCIGN sites using IGS orbits and Earth orientation parameters. We estimated pre- and post-seismic coordinates of LDES from the rigorous combination (using a Kalman filter) of 7 daily solutions before and after the earthquake. We further assumed that the coseismic displacement at LDES occurred as an instantaneous step function.

The static offsets (Table 2) at the other sites are estimated from the single-epoch GPS solutions. We estimate the displacement at each site as the differ-

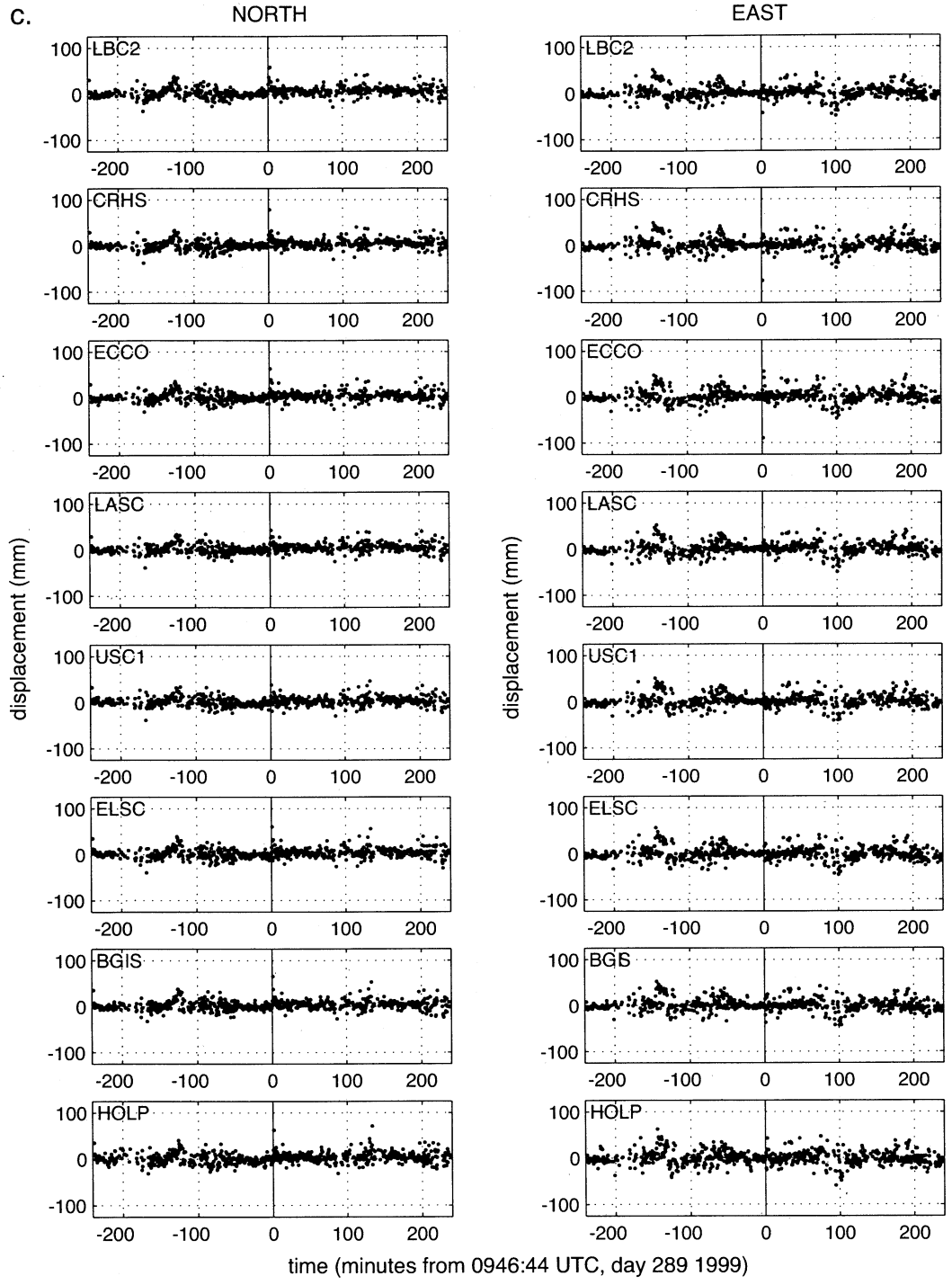

Figure 2. (continued)

ence in medians computed over specified pre- and post-earthquake intervals, in this case, 4 hours (or 480 GPS observation epochs) before and after the earthquake (Figure 2). The observed displacements, with uncertainties of the order of 10 mm, agree with the batch analysis results to within a few millimeters (Table 2, Figure 3). Because we expect some degree of post-seismic deformation at timescales of hours to days, the small differences between the single-epoch and batch analysis offsets may result either from differences in processing technique or from differences in the data interval, 8 hours versus 2 weeks, used for the estimate.

5. Dynamic Displacement

In the first few minutes following the earthquake the GPS observations show a dynamic displacement superimposed on the static component (Figure 4). We modeled the displacement field using the theory of *Aki and Richards* [1980, chapter 4] for a double couple source

Table 2. Comparison of Static Offsets

Site	Epicentral Distance, km	Observed Offset,[a] mm		Observed Minus Daily Analysis Offset Difference,[b] mm		Observed Minus Model Offset Difference,[c] mm	
		North	East	North	East	North	East
LDES	39	179.6 ± 0.8	57.3 ± 0.8	0.0	0.0	−37.6	−29.1
CTMS	53	104.3 ± 0.9	31.7 ± 0.9	−0.7	0.4	−10.0	−0.7
WIDC	74	54.2 ± 0.9	14.8 ± 0.9	1.6	−0.9	−3.1	−0.8
PSAP	88	33.3 ± 0.9	12.1 ± 0.9	1.8	1.0	−8.6	−1.0
PIN1	110	21.5 ± 1.0	5.3 ± 0.9	3.8	−0.9	−4.2	−1.8
AZRY	121	18.9 ± 1.0	4.5 ± 1.0	3.2	−1.2	−3.5	−2.9
PMOB	147	12.3 ± 1.2	3.4 ± 1.1	2.7	−0.5	−2.8	−2.5
MVFD	155	9.8 ± 1.3	2.5 ± 1.2	0.8	0.6	−3.1	−1.1
MONP	189	7.1 ± 1.3	3.9 ± 1.3	3.1	1.4	−1.0	2.0
BBRY	67	27.8 ± 0.9	5.3 ± 1.1	3.2	−0.8	−0.9	−4.6
MSOB	95	11.3 ± 1.0	−2.3 ± 1.2	3.3	−0.1	1.9	0.7
RTHS	114	8.1 ± 1.0	−0.7 ± 1.2	1.7	−2.0	−0.2	−1.8
EWPP	127	6.4 ± 1.0	−0.1 ± 1.2	0.7	0.3	1.1	1.4
CLAR	142	5.8 ± 1.0	−2.0 ± 1.3	1.7	−0.5	2.2	0.7
SPMS	159	6.0 ± 1.1	−0.5 ± 1.3	2.9	−0.3	2.7	0.6
SNHS	169	4.4 ± 1.1	0.3 ± 1.3	1.4	−0.5	1.3	0.9
LBC1	191	5.4 ± 1.3	0.3 ± 1.5	3.4	−1.0	2.9	0.7
LBC2	196	6.6 ± 1.4	0.1 ± 1.7	5.1	−1.1	4.1	0.3
CRHS	202	5.0 ± 1.4	−0.1 ± 1.7	3.6	−1.6	3.0	0.5
ECCO	204	3.9 ± 1.4	1.3 ± 1.8	2.4	−0.3	2.1	2.6
LASC	200	4.8 ± 1.4	1.0 ± 1.7	3.2	0.0	3.0	2.5
USC1	195	3.1 ± 1.4	0.5 ± 1.7	2.1	0.7	1.5	2.8
ELSC	188	4.3 ± 1.4	−1.7 ± 1.8	2.6	−2.1	2.5	0.6
BGIS	186	4.0 ± 1.4	−1.5 ± 1.7	1.9	−2.3	1.9	0.2
HOLP	189	3.5 ± 1.5	−1.6 ± 1.9	0.8	−2.4	1.4	−0.3

[a] Static offsets observed by instantaneous positions are the difference in single-epoch medians, 4 hours before and after the earthquake (except for LDES, where the 2-week daily analysis static offsets and (1-sigma) uncertainties are assumed). Offset uncertainties are computed as the root-sum-square of the pre- and post-earthquake median variances [*Wdowinski et al.*, 1997; *Zhang et al.*, 1997], assuming white noise, and the LDES offset variance.

[b] Daily analysis offsets, compared with observed static offsets, are coseismic displacements estimated using 2 weeks of daily coordinate solutions.

[c] Modeled static offsets, compared with observed offsets, are obtained by doubling the displacement due to a point shear dislocation in an elastic whole space (see text for model details).

in a homogeneous elastic whole space. The total displacement field, $\mathbf{u}(\mathbf{x},t)$, can be expressed as the sum of near-field ($\mathbf{u}^N$), intermediate-field ($\mathbf{u}^I$), and far-field ($\mathbf{u}^F$) terms:

$$\mathbf{u}(\mathbf{x},t) = \mathbf{u}^N(r^{-4},\mathbf{A}^N,M_0) + \mathbf{u}^I(r^{-2},\mathbf{A}^I,M_0) + \mathbf{u}^F(r^{-1},\mathbf{A}^F,dM_0/dt), \quad (1)$$

where M_0 is the time-dependent seismic moment, r is radial distance from the source point, and the $\mathbf{A}$ terms include the effects of the elastic properties and the fault orientation. We assume that the strike is 336°, that the seismic moment rises as a $\sin^2$ function to a moment of 5.98×10^{19} N m (http://www.seismology.harvard.edu), and that the elastic medium is a Poisson solid. Using forward modeling, we determined that a reasonable P wave velocity (6 km/s) and rupture duration (14 s) would provide a good model fit to the observations along the north-south profile. Source time function models of the Hector Mine earthquake indicate that the overall rupture duration is ~17 s [*Dreger and Kaverina*, 2000]. The whole-space model ignores the effects of the free surface, including the amplification of all waves, the phase shift of SV waves with large incident angles, and the presence of SP waves and Rayleigh waves. We account for the free surface by doubling the whole-space displacement amplitude [*Trifunac*, 1974; *Trifunac and Udwadia*, 1974; *Jiao et al.*, 1995], recognizing that this may be an overly simplistic approximation for some displacement components at some incidence angles [*Anderson*, 1976].

The near-, intermediate-, and far-field terms are labeled as such because of their dependence on distance from the source point [*Aki and Richards*, 1980] (equation (1)). The $\mathbf{u}^N$ and $\mathbf{u}^I$ terms combine (Figure 5) to induce a permanent, or static, offset that attenuates as r^{-2}, while the $\mathbf{u}^F$ term attenuates as r^{-1}. The $\mathbf{u}^F$ term only causes a dynamic displacement and becomes more prominent at larger distances, since $\mathbf{u}^N$ and $\mathbf{u}^I$ decay

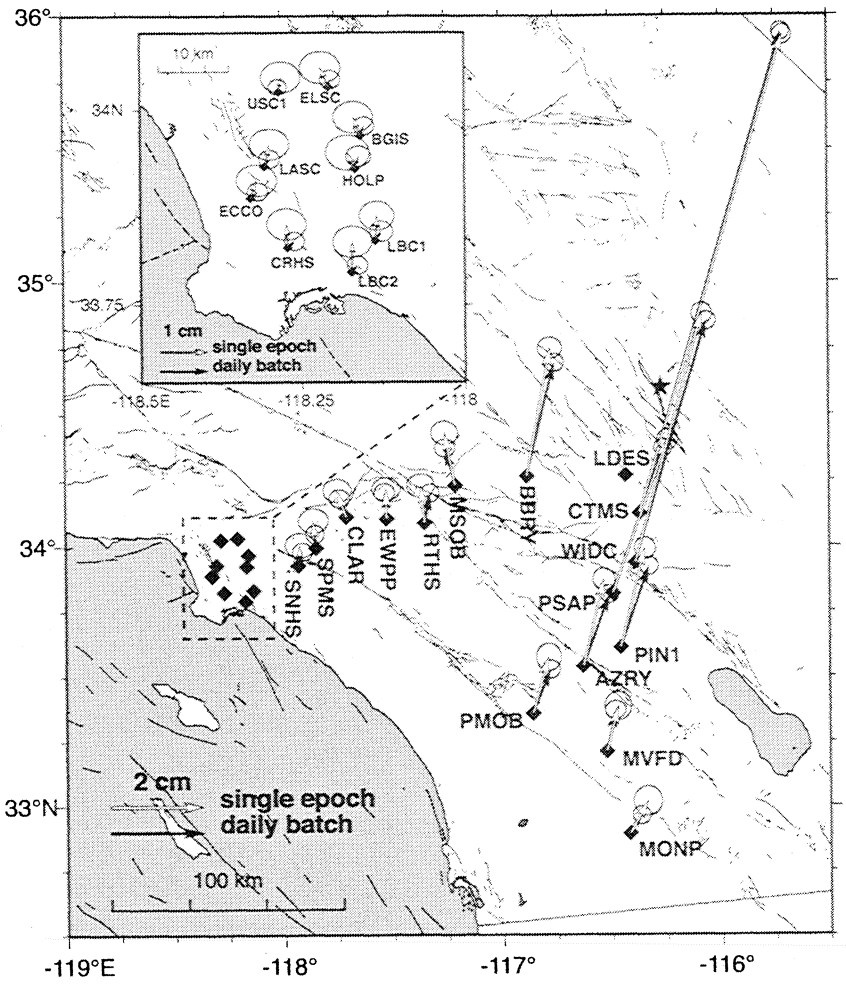

Figure 3. Observed horizontal static coseismic displacements (open arrows), computed as the difference in the 4-hour medians of the pre- and post-earthquake instantaneous GPS solutions, are compared to estimates from the analysis of 2 weeks of daily coordinate solutions (solid arrows). Inset figure shows the displacements at the Los Angeles basin sites. Error ellipses show 95% confidence. The relatively large displacement at LDES (Table 2) is omitted for clarity. The RMS difference between the two static coseismic displacement estimates is 2.8 mm. Data used for this figure are summarized in Table 2.

faster with distance than $\mathbf{u}^F$. The four-lobed radiation pattern of the horizontal static displacement field (Figure 1a), both near and far from the source point, has its largest amplitudes in the radial directions at 45° angles to the fault normal. The radiation pattern of the maximum horizontal displacement field (Figure 1b) is similar close to the source since the near-field (or static) term is dominant. Farther from the source point, however, the maximum displacement is dominated by the dynamic terms, and the displacement field begins to resemble the far-field S wave radiation pattern in which the largest displacements are in the transverse direction.

In spite of the modeling approximations and the relatively sparse GPS observations the overall agreement between the point source model and the data along the north-south profile is good (Figure 6). At LDES, 39 km from the epicenter, the modeled dynamic component occurs well before the second measurement following the earthquake (at 33 s), so that the assumption of a step function displacement at LDES does not affect the estimated displacements at the other sites. At the more distant sites the second and third observations (33 and 63 s) track the arrival of the traveling dynamic wave in both the north and east directions. At Wide Canyon (WIDC), 74 km from the epicenter, both the model and the observations indicate a slight displacement at 33 s in the east direction but not in the north direction. Likewise at Piñon Flat (PIN1), 110 km from the epicenter, both the model and observations show a significant north displacement at 33 s but not an east displacement, since the east dynamic pulse has already passed through. The model even predicts the larger east than north displacement at 63 s at the farthest site, MONP, 189 km from the epicenter.

Our purpose in comparing the single-epoch GPS solutions to modeled displacements is to emphasize the

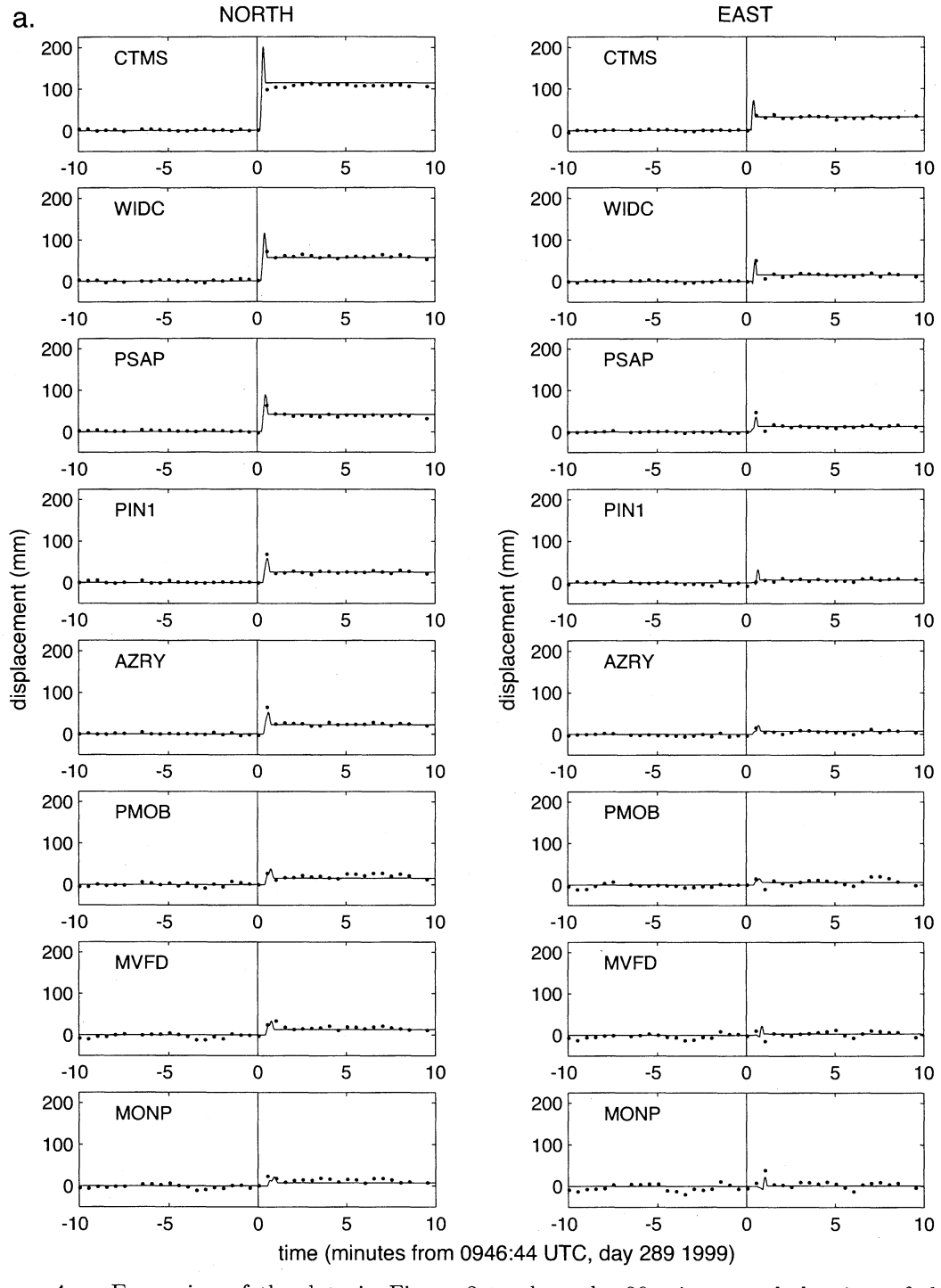

Figure 4. Expansion of the data in Figure 2 to show the 20 min around the time of the earthquake: (a) the north-south profile, (b) east-west profile, and (c) Los Angeles basin sites. The shaded line shows the model displacements.

validity of the GPS data as measures of true ground motion. The agreement of the GPS solutions (for sites external to the Los Angeles basin) with even a simple model suggests that the larger scatter in solutions just after the earthquake reflects actual displacements rather than processing problems. The model that we have chosen, while simple, is sufficient to confirm the geodetic observation of dynamic coseismic deformation.

Moving west from the earthquake toward the Los Angeles basin, the fit to the model deteriorates, and we observe scatter in the postearthquake data that is not predicted for an elastic half-space (Figure 4c). Within the Los Angeles basin the GPS observations show large displacements, with amplitudes of several centimeters, in the 3-4 min following the earthquake. This result is certainly not surprising, considering the extensive history

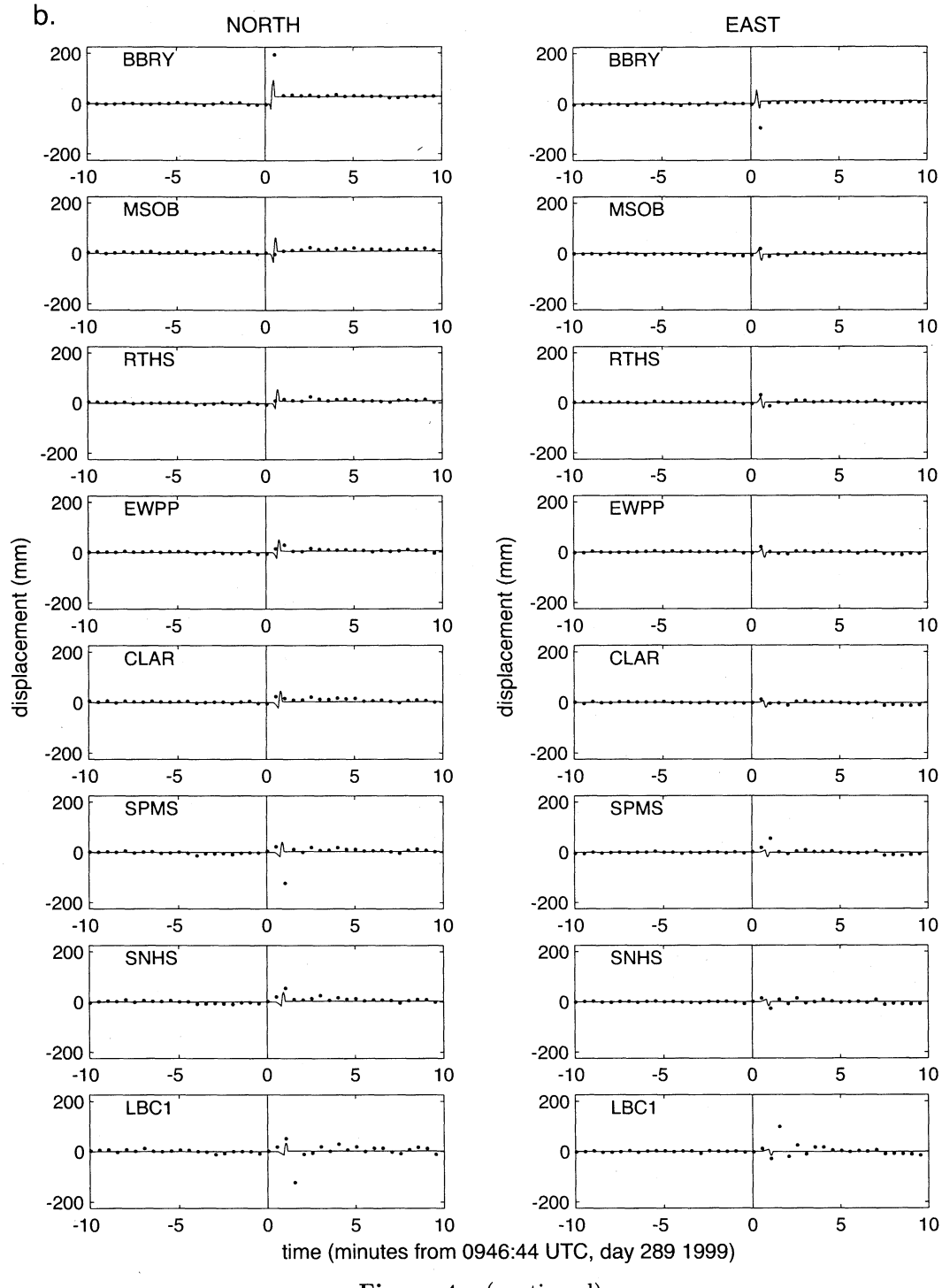

Figure 4. (continued)

of seismic observations showing large-amplitude, long-period resonances in the basin [*Hanks,* 1975; *Rogers et al.,* 1985; *Hartzell et al.,* 1997; *Wald and Graves,* 1998], caused by the trapping and excitation of surface waves in the sedimentary layer [*Liu and Heaton,* 1984]. The trapping of the seismic energy is largely controlled by the underlying basin structure, the basin edge, and the large velocity gradient within the basin [*Vidale and Helmberger,* 1988; *Scrivner and Helmberger,* 1994]. *Wald and Graves* [1998] examined strong motion records from the 1992 Landers earthquake and found that the displacement amplitudes within the basin are ~3 times larger than those outside the basin, with peak displacements >20 cm over the deepest part of the basin (near the SCIGN site Hollydale (HOLP)) (Figure 1c). In section 6, we compare seismic observations recorded for the Hector Mine earthquake with the GPS observations.

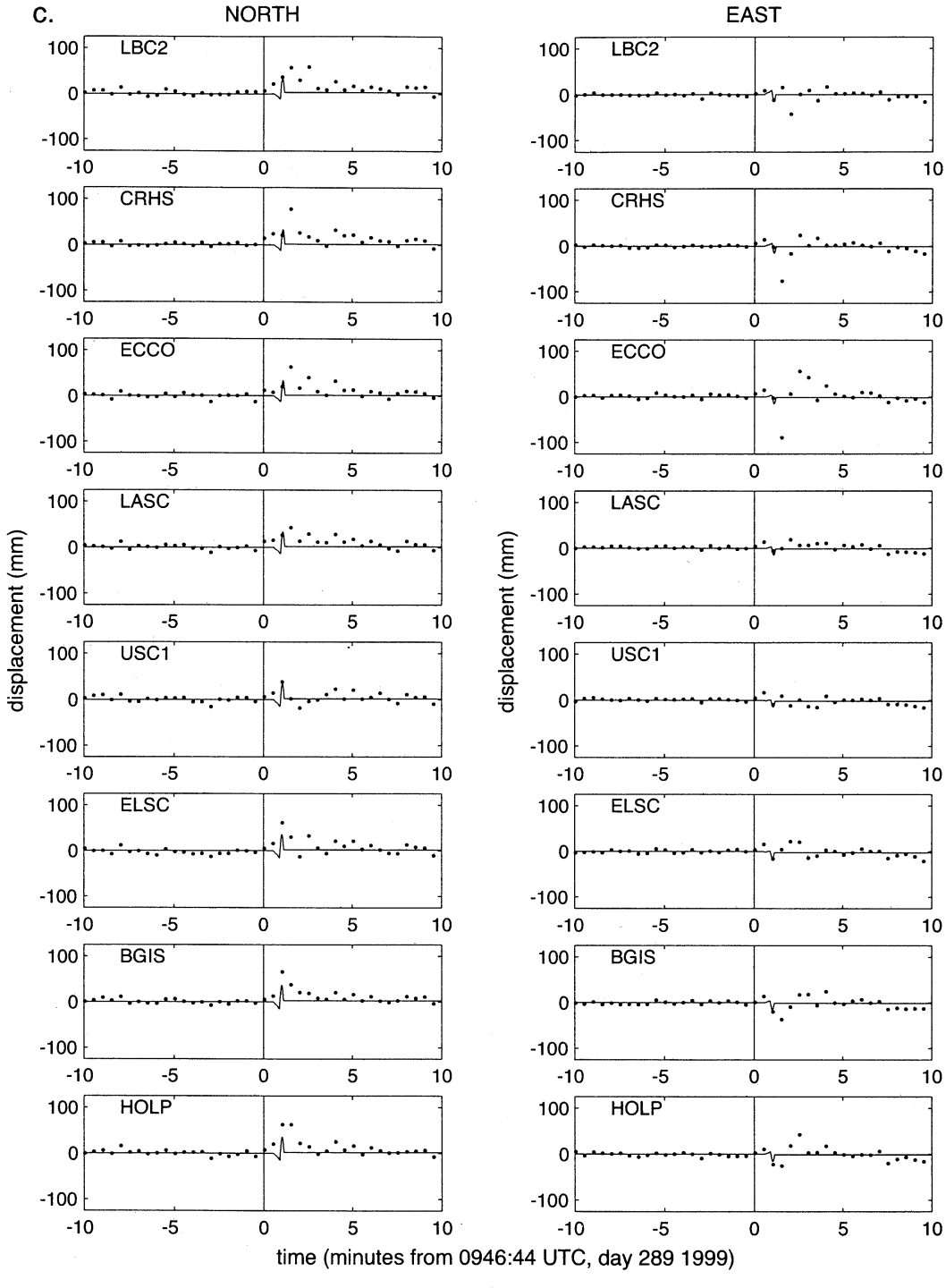

Figure 4. (continued)

6. Comparison With Seismic Data

Ground displacements can be obtained from digital seismic data through integration, or deconvolution, of the records. Because the response of any inertial seismometer to displacement falls to zero at zero frequency, this deconvolution amplifies low frequencies, so the seismic record must generally be high-pass filtered to avoid having the lowest frequencies of the deconvolved record being dominated by noise. How much high-pass filtering is needed depends on the particular instrument and application. For example, to investigate $\geq$2-s ground motions in the Los Angeles basin associated with the Landers earthquake, *Wald and Graves* [1998] applied a band-pass filter with cutoffs at 2 and 17 s to acceleration records from analog SMA-1 strong motion instruments, and found a long-period basin resonance period of $\sim$5 s. Likewise, *Scrivner et al.* [2000] found a long-period basin resonance with a period of 6-7 s in the Hector Mine records, using TriNet (http://www.trinet.org) strong motion data filtered with an Ormsby filter, ramp-

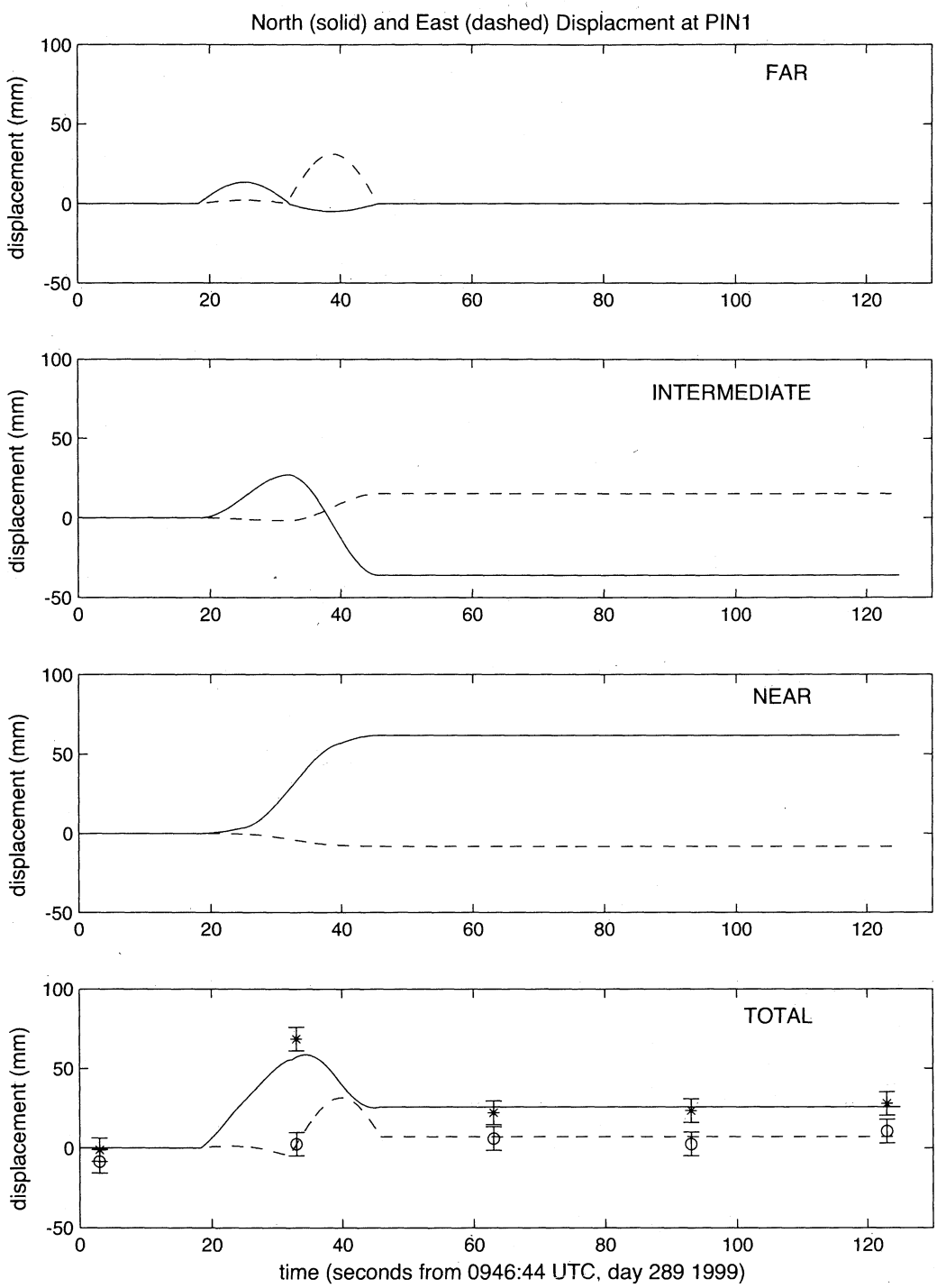

Figure 5. Contributions of far-, intermediate-, and near-field displacements to the (bottom) total modeled displacement in north (solid lines) and east (dashed lines) directions at PIN1, 111 km from the source. North (asterisks) and east (circles) GPS observations, with 95% confidence uncertainties, are plotted with the total displacement. The displacement model is detailed in the text.

ing from zero response at a 25-s period to unity gain at 12.5 s. In both studies the bandwidth of interest, with a period from 5-10 s, was easily recovered from available seismic data.

However, removing any signal with periods greater than a few tens of seconds prohibits the detection of even longer-period features in the seismic data. Given that the GPS observations show large-amplitude ground displacements lasting for more than a few minutes at some locations in the Los Angeles basin, it is likely that lower frequency signals may be a significant contributor to the overall ground displacement, albeit much smaller than the high-frequency component. The deconvolved seismic data and the geodetic data provide comple-

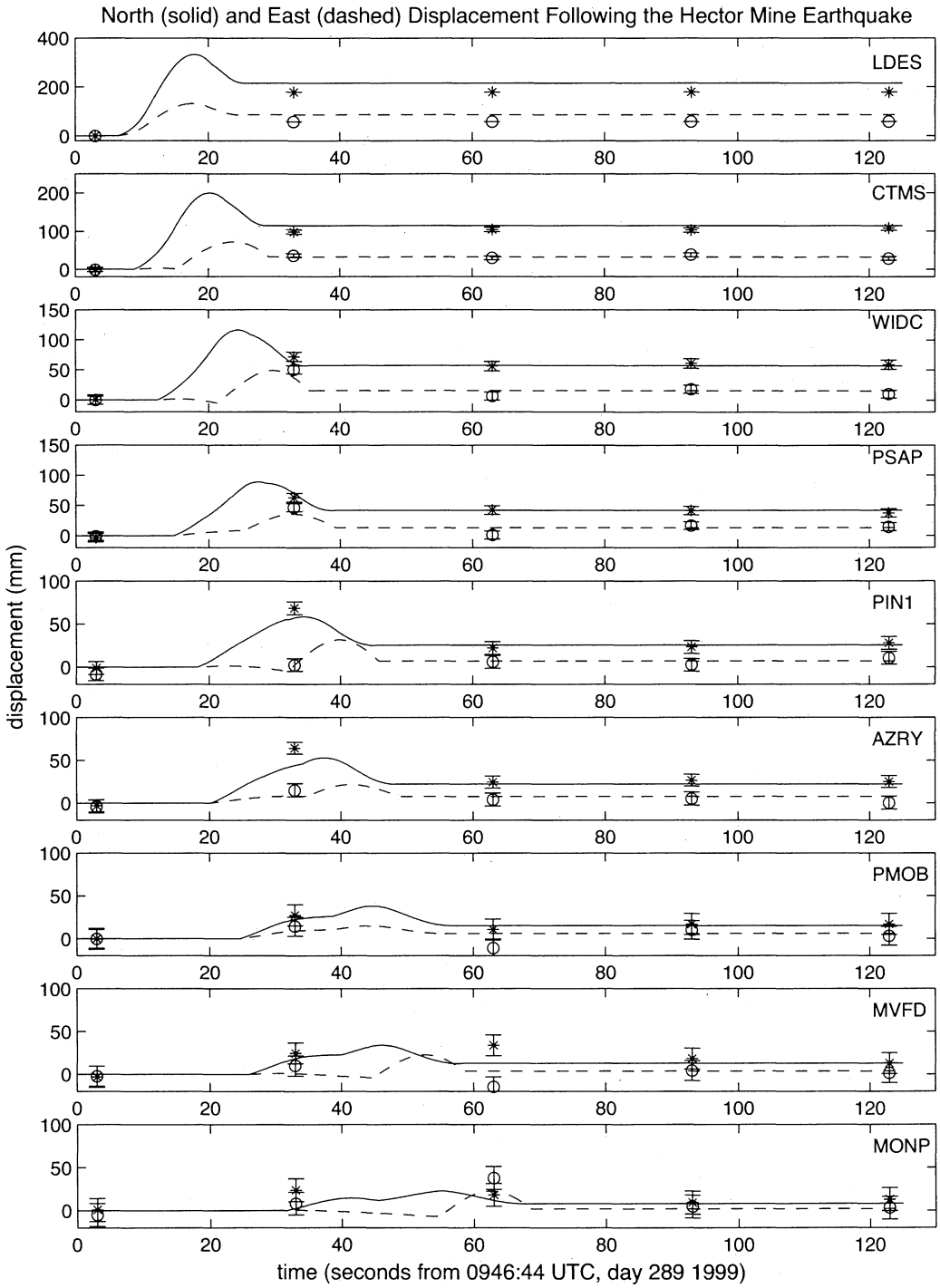

Figure 6. Observed and modeled ground displacements along the north-south profile in north(asterisks and solid lines) and east (circles and dashed lines) directions. The preseismic median at each site is removed, and sites are in order of (top) closest to (bottom) farthest from the epicenter. Error bars show 95% uncertainties.

mentary measurements for detecting seismic ground motions, each providing information over different frequency bands. The 30-s GPS sample interval is insufficient for analysis in the frequency domain or, probably, for formal combination of measurement types (e.g., in a Kalman filter). Instead, we demonstrate the use of the GPS measurements to constrain the seismic data at long periods, and we compare the single-epoch GPS observations with colocated seismic data at selected sites in the Los Angeles basin.

The GPS solutions can serve as long-period constraints for the deconvolution of seismic accelerations (Figure 7). At the Piñon Flat Observatory, a Kinemetrics FBA-23 (force balance accelerometer), which is located at the Incorporated Research Institutions for Seismology / International Deployment of Accelerometers

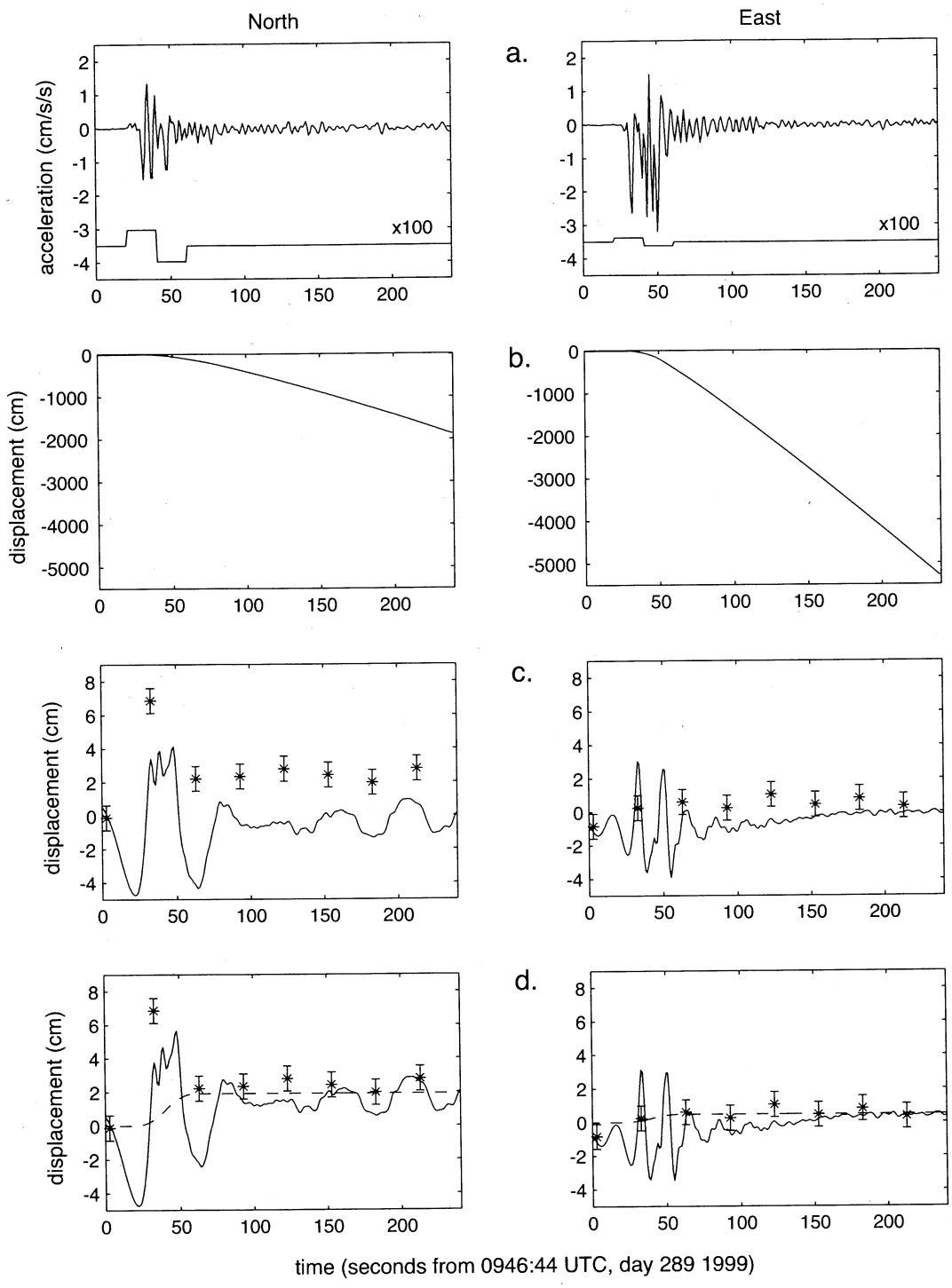

Figure 7. Strong motion data at Piñon Flat Observatory as measured by a Kinemetrics FBA-23 (force balance accelerometer) at the Incorporated Research Institutions for Seismology / International Deployment of Accelerometers seismic station PFO. (a) Acceleration data sampled at 1 Hz (top line). (b) Twice-integrated accelerations without high-pass filtering. (c) Displacements computed from high-pass filtered accelerations, with cutoffs at 60 s and 20 s for the north and east components, respectively, compared with permanent displacements observed by the GPS data (asterisks with 95% confidence error bars). An acceleration correction signal (7a, bottom line), designed to counter sensor anomalies related to transducer hysteresis (see text), is twice integrated to generate a long-period displacement correction signal (7d, dashed line). (d) Application of the correction signal. This forces the seismic displacement (solid line) to fit the GPS observations (asterisks).

seismic station PFO (http://www.fdsn.org/station_book/II/PFO/pfo.html), recorded strong motions 140 m from the SCIGN site, PIN1 (Figure 7a, top line). Double integration of the measured accelerations (with the preearthquake baseline removed) leads to unreasonably large displacements (Figure 7b). We applied a high-pass filter, with cutoff periods at 60 s for the north component and 20 s for the east component, to the acceleration data to mitigate the effect of long-period instrument instabilities. Application of the high-pass filter eliminates the large drift in displacement but also eliminates the permanent 2-cm (north) displacement apparent in the GPS signal (Figure 7c).

Since the filtered seismic data offers displacement information only at high frequencies, we are free to alter the signal at long periods to force a fit to the GPS measurements. A long-period correction signal (Figure 7d, dashed line) can be combined with the high-pass-filtered seismic displacement (Figure 7c) to create a corrected displacement signal that is consistent with both the measured seismic accelerations at high frequencies and the measured GPS displacements at lower frequencies (Figure 7d).

The displacement correction signal (Figure 7d, dashed line) is the double integral of an acceleration correction signal (Figure 7a, bottom line), designed to counter the effects of mechanical and/or electrical transducer hysteresis [*Iwan et al.*, 1985]. Minute baseline shifts in the transducer output occur upon arrival of very large acceleration pulses. We constructed the acceleration correction signal as a sequence of small acceleration offsets, with magnitudes on the order of 1000^{-1} of the measured accelerations, applied during the strongest part of the acceleration record [*Iwan et al.*, 1985]. The offset magnitudes are computed using

$$\mathbf{d} = \tfrac{1}{2}\mathbf{a}t^2, \tag{2}$$

where $\mathbf{d}$ are the north and east static displacements observed with GPS, $\mathbf{a}$ are the solved-for magnitudes of the north and east acceleration corrections, and t is roughly the duration of large-amplitude accelerations that require correction. We chose a value of t, 30 s, and positioned the offsets by trial and error so that after double integration the displacement record would have a long-period shape that matches the GPS observations (Figure 7d).

The above example demonstrates that the complementary measurements can be used to recover a more complete record of ground displacement, compared with the ground displacement signal from either of the individual techniques. Here we used only the GPS static offset, along with the elementary assumption that the offset develops smoothly in time, to constrain the seismic data. The high-rate GPS data were not actually used in the correction. A more elaborate solution might involve the formal estimation, for example, using weighted least squares, to best fit the seismic observations to more frequent GPS observations.

Next we compare single-epoch GPS measurements (0.033 Hz) with strong motion accelerations (100 Hz) recorded by TriNet [*Scrivner et al.*, 2000], which is administered by the California Strong Motion Instrumentation Program, Caltech, and the U.S. Geological Survey (Figure 8). The triggered strong motion records, recorded at 100 Hz, span only a few minutes so that there are at most 4 coincident GPS measurements on each record. Broadband seismic instruments (e.g., Terrascope (http://www.scecdc.scec.org/terra.html)) that recorded in Los Angeles during the Hector Mine event offer longer, or even continuous, spans of data; however, these instruments generally went off scale (or "clipped") upon arrival of the surface waves, making them unusable for computation of ground displacement.

We chose data from three TriNet sites that are situated close to SCIGN sites in the Los Angeles basin (Figure 1c) and that exhibited large-amplitude displacements. In each case we observe that the GPS measurements underestimate the peak displacement observed by the seismic instruments. For example, at Downey, near the deepest part of the basin [*Wald and Graves*, 1998] and the site of the largest displacements in both the geodetic (HOLP) and seismic (DOW) data sets, the GPS displacement peaks at ~7 cm in the north-south direction, while the strong motion displacement reaches nearly 20 cm. We also observe that the GPS observations continue to show significant displacements for a longer duration than is shown by the seismic data, such as the east-west component at DOW. These two observations underscore the complementary nature of the two measurement techniques: The seismic data track ground motion for a short span with very high temporal resolution, while the GPS data track ground motion at lower frequencies for longer durations.

During the Hector Mine earthquake the SCIGN receivers were operating at the standard 0.033-Hz sampling rate of continuous GPS arrays. Therefore our data are temporally aliased with respect to periods shorter than the Nyquist period of 60 s. This aliasing does not appear to cause significant problems in fitting displacement data along the north-south profile (Figure 4a), implying that the underlying source-time function for the Hector Mine event is fairly smooth in displacement. However, our GPS data are clearly undersampled with respect to the basin resonances shown in Figure 8. In this case a higher GPS sample rate would be very helpful.

7. Summary

We have demonstrated that the dynamic ground displacements predicted for a large earthquake can be directly measured with instantaneous GPS positioning. We have also demonstrated that the single-epoch GPS observations show large-amplitude, long-duration displacements consistent with what is known to occur in the Los Angeles basin. These results were made possible by advances in GPS positioning (instantaneous phase

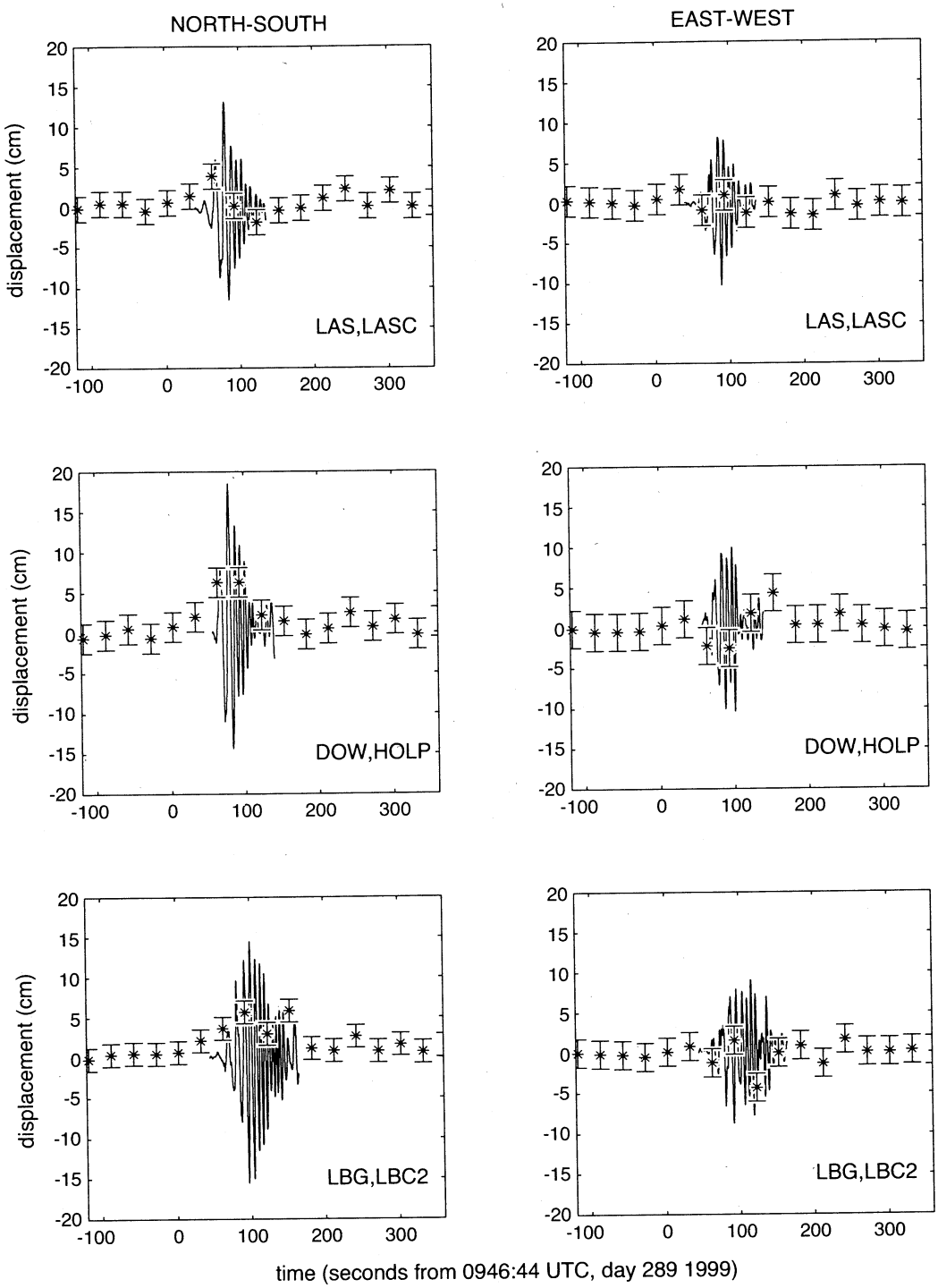

Figure 8. Comparison of single-epoch GPS solutions (0.033 Hz) with twice-integrated TriNet strong motion data (100 Hz) in the north-south and east-west directions at three locations (TriNet/GPS): Los Angeles (LAS/LASC), Downey (DOW/HOLP), and Long Beach (LBG/LBC2). Error bars on GPS data show 95% confidence. TriNet accelerations have been band-pass filtered with an Ormsby filter, ramping from zero response at 1/(25 s) to unity gain at 1/(12.5 s), before double integration to displacement.

ambiguity resolution algorithms), the existence of the SCIGN array of GPS receivers, and the well-placed M_w 7.1 Hector Mine earthquake. During the Hector Mine earthquake the SCIGN receivers collected phase measurements every 30 s. From these measurements we generated coordinate solutions every 30 s for 24 SCIGN receivers and showed that the displacements outside of the Los Angeles basin follow those predicted by a simple elastic half-space model. Within the Los Angeles basin we observe displacements with amplitudes up to several centimeters that last for as much as 3 - 4 min. These results suggest that GPS is a valuable method for measur-

ing long-period displacements that were, until recently, observed only with traditional seismic instruments.

A higher GPS sample rate would have provided better temporal resolution. In principle, the rate of single-epoch GPS solutions is limited only by the receiver sampling rate, which is 2 Hz for the SCIGN receivers. The dynamic response of the GPS receivers appears to be adequate for tracking seismic ground motions at rates of at least 1 Hz, although further analysis of the time correlation of the GPS measurements at very high frequencies (1-10 Hz) is warranted. Our analysis of the Hector Mine earthquake demonstrates that a higher sample rate should be seriously considered for existing continuous GPS arrays and for future deployments in seismically active regions, such as the proposed Western North America Plate Boundary Observatory [*Silver et al.,* 1999]. We have shown that even at current sampling rates, GPS can provide valuable measurements of long period ground motions, hence narrowing the frequency gap between seismology and geodesy.

Acknowledgments. This research was supported by the Southern California Earthquake Center. SCEC is funded by NSF Cooperative Agreement EAR-8920136 and USGS Cooperative Agreements 14-08-0001-A0899 and 1434-HQ-97AG01718. The SCEC contribution number for this paper is 578. We acknowledge the Southern California Integrated GPS Network and its funders (W.M. Keck Foundation, NASA, NSF, USGS, and SCEC) for providing data used in this study. We are grateful to Pete Davis for his assistance in obtaining the Piñon Flat IRIS data. Thoughtful reviews by David Wald and Bill Ellsworth helped to improve the manuscript.

References

Aki, K., and P. G. Richards, *Quantitative Seismology: Theory and Methods,* W. H. Freeman New York, 1980.

Anderson, J. G., Motions near a shallow rupturing fault: Evaluation of effects due to the free surface, *Geophys. J. R. Astron. Soc., 46,* 575-593, 1976.

Anderson, J. G., et al., Strong ground motion from the Michoacan, Mexico, earthquake, *Science, 233,* 1043-1049, 1986.

Blewitt, G., et al., Absolute far-field displacements from the June 28, 1992, Landers earthquake sequence, *Nature, 361,* 340-342, 1993.

Bock, Y., et al., Detection of crustal deformation from the Landers earthquake sequence using continuous geodetic measurements, *Nature, 361,* 337-340, 1993.

Bock, Y., et al., Southern California Permanent GPS Geodetic Array: Continuous measurements of the regional crustal deformation between the 1992 Landers and 1994 Northridge earthquakes, *J. Geophys. Res., 102,* 18,013-18,033, 1997.

Bock, Y., R. M. Nikolaidis, P. J. de Jonge, and M. Bevis, Instantaneous geodetic positioning at medium distances with the Global Positioning System, *J. Geophys. Res., 105,* 28,223-28,253, 2000.

Bona, P., Precision, cross correlation and time correlation of GPS phase and code observations, *GPS Solutions, 4,* 2, 3-13, 2000.

Boucher, C., Z. Altamimi, and P. Sillard (eds.), The 1997 International Terrestrial Reference Frame, *IERS Tech. Note 27,* Int. Earth Rotation Serv., Paris, 1997.

Dreger, D., and A. Kaverina, Seismic remote sensing for the earthquake source process and near-source strong shaking: A case study of the October 16, 1999 Hector Mine earthquake, *Geophys. Res. Lett., 27,* 1941-1944, 2000.

Ekstrom, G., Calculation of static deformation following the Bolivia earthquake by summation of Earth's normal modes, *Geophys. Res. Lett., 22,* 2289-2292, 1995.

Ge, L., GPS seismometer and its signal extraction, paper presented at 12th International Meeting of the Satellite Division of the U.S. Institute of Navigation, Nashville, 1999.

Ge, L., L. Dai, S. Han, C. Rizos, Y. Ishikawa, and Y. Yoshida, GPS seismometers: the implementing issues, paper presented at 13th International Meeting of the Satellite Division of the U.S. Institute of Navigation, Salt Lake City, 2000.

Gourevitch, S., Measuring GPS receiver performance: A new approach, *GPS World,* 56-62, 1996.

Hanks, T. C., Strong ground motion of the San Fernando, California, earthquake: Ground displacements, *Bull. Seismol. Soc. Am., 65,* 193-225, 1975.

Hartzell, S., E. Cranswick, A. Frankel, D. Carver, and M. Meremonte, Variability of site response in the Los Angeles urban area, *Bull. Seismol. Soc. Am., 87,* 1377-1400, 1997.

Hatanaka, Y., T. Hiromichi, A. Yoshiaki, Y. Iimura, K. Kobayashi, and H. Morishita, Coseismic crustal displacements from the 1994 Hokkaido-Toho-Oki earthquake revealed by a nationwide continuous GPS array in Japan - Results of GPS kinematic analysis (in Japanese), paper presented at the Japanese Symposium on GPS, National Committee for Geodesy, Science Council of Japan, and GPS Consortium of Japan, Tokyo, 1994.

Hatanaka, Y., H. Tsuji, Y. Iimura, K. Kobayashi, and H. Morishita, Application of GPS kinematic method for detection of the crustal movements with high temporal resolution, in *IAG Symposia,* vol. 115, edited by G. Beutler et al., pp. 105-109, Springer-Verlag, New York, 1995.

Hirahara, K., T. Nakano, Y. Hoso, S. Matsuo, and K. Obana, An experiment for GPS strain seismometer, paper presented at the Japanese Symposium on GPS, National Committee for Geodesy, Science Council of Japan, and GPS Consortium of Japan, Tokyo, 1994.

Iwan, W. D., M. A. Moser, and C. Peng, Some observations on strong-motion earthquake measurement using a digital accelerograph, *Bull. Seismol. Soc. Am., 75,* 1225-1246, 1985.

Jiao, W., T. C. Wallace, S. L. Beck, P. G. Silver, and G. Zandt, Evidence for static displacements from the June 9, 1994, deep Bolivian earthquake, *Geophys. Res. Lett., 22,* 2285-2288, 1995.

Liu, H., and T. H. Heaton, Array analysis of the ground velocities and accelerations from the 1971 San Fernando, California, earthquake, *Bull. Seismol. Soc. Am., 74,* 1951-1968, 1984.

Miyazaki, S., H. Tsuji, Y. Hatanaka, Y. Abe, A. Yoshimura, K. Kamada, K. Kobayashi, H. Morishita, and Y. Iimura, Establishment of the nationwide GPS array (GRAPES) and its initial results on the crustal deformation of Japan, *Bull. Geogr. Surv. Inst., 42,* 27-41, 1996.

Miyazaki, S., Y. Hatanaka, T. Sagiya, and T. Tada, The nationwide GPS array as an earth observation system, *Bull. Geogr. Surv. Inst., 44,* 11-22, 1998.

Rogers, A. M., J. C. Tinsley, and R. D. Borcherdt, Predicting relative ground motion response, in *Evaluating Earthquake Hazards in the Los Angeles Region - An Earth-Science Perspective, U.S. Geol. Surv. Prof. Pap., 1360,* 1985.

Scrivner, C. V., and D. V. Helmberger, Seismic waveform

modeling in the Los Angeles basin, *Bull. Seismol. Soc. Am., 84,* 1310-1326, 1994.

Scrivner, C. W., V. Graizer, A. Shakal, and T. Cao, TriNet strong-motion data from the M7.1 Hector Mine, California, earthquake: Ground motions in the Los Angeles basin, *Seismol. Res. Lett., 71,* 226, 2000.

Silver, P. G., et al., A Plate Boundary Observatory, *IRIS Newsl., XVI,* 3,7-9, 1999.

Tada T., T. Sagiya, and S. Miyazaki, Deformation of Japan Islands viewed by GPS (in Japanese), *Kagaku, 67,*(12), 917-927, 1997.

Tiberius, C. C. J. M., The GPS data weight matrix: What are the issues?, paper presented at the National Technical Meeting, Institute of Navigation, San Diego, Calif., 1999.

Trifunac, M. D., A three-dimensional dislocation model for the San Fernando, California, earthquake of February 9, 1971, *Bull. Seismol. Soc. Am., 64,* 149-172, 1974.

Trifunac, M. D., and F. E. Udwadia, Parkfield, California, earthquake of June 27, 1966: A three dimensional moving dislocation model, *Bull. Seismol. Soc. Am., 64,* 511-533, 1974.

Urhammer, R., L. S. Gee, M. Murray, D. Dreger, and B. Romanowicz, The M_w 5.1 San Juan Bautista, California, earthquake of 12 August 1998, *Seismol. Res. Lett., 70,* 10-18, 1999.

U.S. Geological Survey, Southern California Earthquake Center, and California Division of Mines and Geology: Preliminary report on the 10/16/1999 M7.1 Hector Mine, California earthquake, *Seismol. Res. Lett., 71,* 11-23, 2000.

vanDam, T., G. Mader, and M. Schenewerk, GPS detects co-seismic and post-seismic surface displacements caused by the Northridge earthquake, *Eos Trans. AGU, 75*(16), Spring Meet. Suppl., 103, 1994.

Vidale, J. E., and D. V. Helmberger, Elastic finite-difference modeling of the 1971 San Fernando, California, earthquake, *Bull. Seismol. Soc. Am., 78,* 122-141, 1988.

Vidale, J., S. Goes, and P. G. Richards, Near-field deformation seen on distant broadband seismograms, *Geophys. Res. Lett., 22,* 1-4, 1995.

Wald, D., and R. Graves, The seismic response of the Los Angeles basin, California, *Bull. Seismol. Soc. Am., 88,* 337-356, 1998.

Wdowinski, S., Y. Bock, J. Zhang, P. Fang, and J. F. Genrich, Southern California Permanent GPS Geodetic Array: Spatial filtering of daily positions for estimating coseismic and postseismic displacements induced by the 1992 Landers earthquake. *J. Geophys. Res., 102,* 18,057-18,070, 1997.

Zhang, J., et al., Southern California Permanent GPS Geodetic Array: Error analysis of daily position estimates and site velocities, *J. Geophys. Res., 102,* 18,035-18,055, 1997.

D. Agnew, Y. Bock, P. J. de Jonge, R. Nikolaidis, P. Shearer, and M. Van Domselaar, Cecil H. and Ida M. Green Institute of Geophysics and Planetary Physics, Scripps Institution of Oceanography, La Jolla, CA 92093, USA. (agnew@ramsden.ucsd.edu; ybock@ucsd.edu; paul@hotmail.com; rosanne@ucsd.edu; pshearer@ucsd.edu; matthijs@josh.ucsd.edu)

(Received July 17, 2000; revised June 8, 2001; accepted June 9, 2001.)